Macromolecular Research, Vol. 22, No. 5, pp 509-514 (2014)
DOI 10.1007/s13233-014-2071-4

www.springer.com/13233
pISSN 1598-5032 eISSN 2092-7673

Carbon Aerogels Based on Regenerated Silk Proteins and Graphene Oxide for Supercapacitors

Young Soo Yun, Se Youn Cho, and Hyoung-Joon Jin*

Department of Polymer Science and Engineering, Inha University, Incheon 402-751, Korea

Received September 17, 2013; Revised January 21, 2014; Accepted January 29, 2014

Abstract: Carbon aerogels based on regenerated silk proteins and graphene oxide (GO) were prepared by a flash freezing/lyophilization process followed by carbonization. Hydrophilic blocks of ampiphilic silk proteins showed strong interactions with the oxygen functional groups of GO through intermolecular hydrogen bonds, resulting in silk-protein-coated GO nanoplates. The silk-protein-coated GO nanoplates were assembled into 3D cryogels by the gelation of the silk proteins after a flash freezing/lyophilization process. The cryogels based on GO and silk proteins, which contained numerous nitrogen heteroatoms, were successfully transformed to carbon aerogels after crystallization by a methanol treatment. Consequently, the nitrogen-enriched carbon aerogels exhibited a high capacitance of 298 F/g because of significant contributions from the pseudocapacitive effects. A specific energy of 63 W h/kg, specific power of 20 kW/kg, and stable cycle life of over 5,000 cycles were achieved.

Keywords: silk, graphene oxide, aerogel, supercapacitor, hybrid, carbonization.

Introduction

Silk produced by the *Bombyx mori* silk worm is one of the most abundant polymers in nature, with global production amounting to more than 480,000 ton per year.[1] Silk fibroin has been extensively studied as a biomaterial.[2] A growing interest on silk fibroin toward fabricating optical and electronic devices has resulted in widespread investigations outside of the textile world.[3-5] Silk fibroin has been dissolved and subsequently reformulated into new materials with various structures and morphological characteristics. In particular, silk fibroin in the sol state can interact with both hydrophobic and hydrophilic materials owing to its amphiphilic properties,[6,7] which make it possible to design new nanostructures from silk fibroin by spontaneous interactions between the heterocomponents.[8] In addition, nanostructured carbon aerogels can be prepared by carbonization of the nanostructured precursors.[9-11] Many researchers have reported the carbonization of silk fibroins.[12-15] However, there are very few reports on carbon materials prepared from regenerated silk fibroin. The paper is, to the best of our knowledge, the first report on the synthesis of carbon materials from regenerated silk in which the proteins are obtained exhibit high electrochemical performance as supercapacitors.[16] The results suggest that silk proteins can be effective precursors for carbon materials that can be used as supercapacitor electrodes.

Graphene, a new class of two-dimensional carbon nanostructure, has attracted enormous interest for various applications owing to its unique physical properties such as high electron mobility (15,000 $cm^2 V^{-1} s^{-1}$), high mechanical strength (>1,060 GPa), high thermal conductivity (~3,000 $W m^{-1} K^{-1}$), and high specific surface area (2,600 $m^2 g^{-1}$).[17-20] Ruoff *et al*. have reported chemically modified graphene-based supercapacitors with capacitances of 135 and 99 F g^{-1} in aqueous and organic electrolytes, respectively.[21] The capacitance values can be increased with greater morphological control or by applying various treatments on graphene.[22-24] In addition, nitrogen-doped graphene has shown capacitance values of ~280 F g^{-1}, contributed by both the conventional electrical double-layer capacitance near the electrode surfaces and the pseudocapacitance of the electroactive nitrogen atoms.[25] In this context, graphene-based nanostructured materials comprising electroactive heteroatoms can be expected to act as excellent electrode materials for supercapacitors. Recently, several papers have described graphene-based aerogels.[26-30] Müllen *et al*. reported three-dimensional graphene-based frameworks (3D-GFs) with hierarchical macroporous and mesoporous structures for supercapacitors.[28] The 3D-GFs exhibited a capacitance value of 226 F/g and stability over 5,000 cycles. They also reported the application of three-dimensional nitrogen and boron co-doped graphene in supercapacitors. However, only a few reports on electrode materials for supercapacitors have been published.[28,31]

In this study, carbon aerogels based on regenerated silk proteins and graphene oxide (GO) (SF-GO carbon aerogel) were prepared. The regenerated silk proteins were success-

*Corresponding Author. E-mail: hjjin@inha.ac.kr

fully transformed into nanostructured carbon materials with GO by a flash freezing/lyophilization process followed by carbonization. Interestingly, the carbon materials from the regenerated silk proteins possessed numerous heteroatoms such as nitrogen and oxygen, which affected the electrochemical performances of the SF-GO carbon aerogels. The enhanced electrochemical performances were caused by various effects from silk protein-induced carbons such as numerous nitrogen and oxygen contents, electroactive nitrogen configurations, rough surface morphology and topography advantageous in wettability with electrolytes. As a result, SF-GO carbon aerogels exhibiting good electrochemical performances were achieved by a simple process based on the regenerated silk proteins and GO.

Experimental

Preparation of GO and Regenerated Silk Fibroin. GO was prepared from natural graphite (Sigma-Aldrich) using the Hummers method. Aqueous GO suspensions were frozen in liquid nitrogen and then freeze-dried using a lyophilizer (LP3, Jouan, France) at 50 ºC and 0.045 mbar for 72 h. Consequently, low-density, loosely packed GO powders were obtained.[32] Aqueous silk fibroin solution was prepared by the following protocol. First, seven cocoons were boiled for 30 min in an aqueous solution of 0.02 M Na_2CO_3 (OCI Company Ltd., 99%, 0.02 M) and rinsed thoroughly with water to extract the glue-like sericin proteins. The extracted silk was then dissolved in a 9.3-M LiBr (Sigma-Aldrich, ≥99%) solution at room temperature to yield a 20 wt% solution. This solution was dialyzed in water using Slide-a-Lyzer dialysis cassettes (Pierce, MWCO 3500) for 36 h. The final concentration of the aqueous silk solution was 7.0-8.0 wt%.[7]

Preparation of SF-GO Carbon Aerogels. A sample comprising 60 mg GO powder was exfoliated by ultrasonication in 40 mL of distilled water at pH 12. The pH was controlled by adding a solution of dilute aqueous NaOH. Then, the GO dispersions were mixed with 40 mg of the regenerated silk fibroin in aqueous solution (10 mL) at pH 12. The mixture was stirred for 1 h, frozen in liquid nitrogen, and freeze-dried using the lyophilizer at -50 ºC and 0.045 mbar for 72 h. The obtained cryogel consisted of 60 wt% of GO and 40 wt% of regenerated silk fibroin. Cryogels with different GO and regenerated silk fibroin weight ratios such as 8:2, 4:6, and 2:8 were prepared by similar methods. The cryogels were treated with methanol vapor at room temperature for 6 h and then heated from room temperature to 800 ºC at a heating rate of 10 ºC/min under a N_2 flow rate of 200 mL/min. Then, the samples were held at 800 ºC for 2 h. The cryogels with GO and regenerated silk fibroin weight ratios of 8:2, 6:4, 4:6, and 2:8 were designated as cryogel-8:2, cyrogel-6:4, cryogel-4:6, and cryogel-2:8, respectively. This notation is used throughout the paper.

Characterization. The morphologies of samples were characterized by field emission scanning electron microscopy (FESEM, S-4300, Hitachi, Japan). The surface elemental composition of the samples was analyzed by X-ray photoelectron spectroscopy (XPS, AXIS-HIS, Kratos Analytical, Japan) with a dual-chromatic MgK_α X-ray source at 1500 eV. X-ray diffraction (XRD, Rigaku, DMAX-2500, Japan) was used to characterize the samples. For Raman spectroscopy, a continuous-wave linearly polarized laser with a wavelength of 514 nm (2.62 eV), pinhole of 50 μm, and 600 grooves mm^{-1} grating were used. To ensure nondestructive measurements, low laser power was used (<300 μW) on the sample. The porous properties of samples were analyzed using nitrogen adsorption and desorption isotherms, which were obtained using a porosimetry analyzer (ASAP 2020, Micromeritics, USA) at -196 ºC. The surface areas (S_{BET}) were calculated according to Brunauer-Emmett-Teller (BET) theory. The mesopore surface area (S_{meso}) was calculated according to the Barrett-Joyner-Halenda (BJH) theory.

The electrodes for the electrochemical tests were prepared as follows: the samples and polytetrafluoroethylene (a binder) were mixed with a mass ratio of 9:1, coated onto a nickel mesh substrate (1×1 cm^2), and dried at 110 ºC for several hours. Each electrode contained approximately 3-4 mg of the electroactive materials. Electrochemical measurements were performed in a three-electrode system and a two-electrode cell configuration. For the three-electrode system, samples containing nickel mesh, platinum plate, and saturated KCl were used as the working, counter, and reference electrodes, respectively. For the two-electrode cell, each electrode had a diameter of 1 cm and a thickness of approximately 100 μm. A typical pair of electrodes had a weight of 2.5-3.0 mg after drying overnight at 100 ºC, and 1 M H_2SO_4 (OCI Company Ltd., 95%) was used as an aqueous electrolyte. The electrodes and a porous polypropylene separator (Whatman GF/D) were sandwiched in a stainless steel cell for the fully assembled two-electrode cell device. Electrochemical data were obtained using cyclic voltammetry and chronopotentiometry (PGSTAT302N, Autolab). Cyclic voltammetry tests were performed between 0 and 1 V at different scan rates. The capacitance, energy density, and power density were all characterized by galvanostatic measurements. A current ranging from 0.5 to 20 A g^{-1} was applied. For the cycling test, a current density of 3 A g^{-1} was applied. Specific capacitances were obtained from cyclic voltammetry plots as follows. Specific capacitances were obtained from galvanostatic charge/discharge curves as follows $C_s = I\Delta t/m\Delta V$. Where, C_s is specific capacitance (F g^{-1}), m is mass of the electroactive materials (g), I is the discharge current (mA), t is the discharge time (t) and ΔV is potential window (V).

Results and Discussion

Silk fibroin exhibits amphiphilic block copolymer-like properties because it is composed of relatively large hydro-

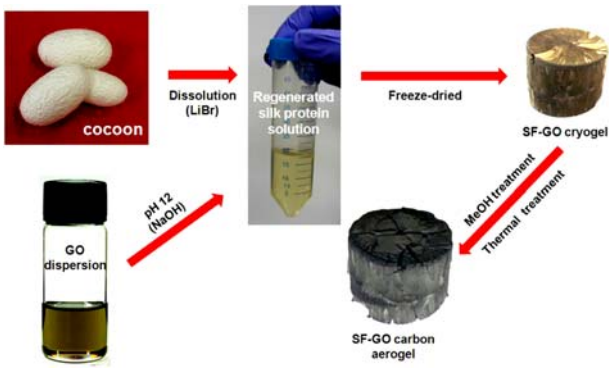

Figure 1. Schematic process for preparing SF-GO carbon aerogels.

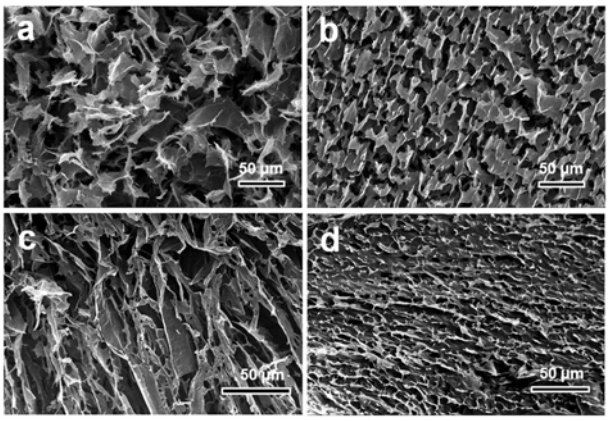

Figure 3. SEM images of (a) cryogel-8:2, (b) cryogel-6:4, (c) cryogel-4:6, and (d) cryogel-2:8.

philic chain end blocks with smaller hydrophilic internal blocks and large internal hydrophobic blocks, where the repeats listed above are encoded.[7] The hydrophilic blocks of the silk fibroin molecules interact strongly with the oxygen functional groups of GO through intermolecular hydrogen bonds. Figure 1 shows the schematic of the process used for preparing the SF-GO carbon aerogels. The regenerated silk fibroin solution is metastable and gelates easily. However, high pH conditions allow the regenerated silk fibroin solution to become stable. Therefore, the solution was mixed with the GO dispersion at pH 12. The SF-GO cryogels were obtained after freeze-drying. In this process, silk fibroins acted as binders assisting the assembly of the GO-based network. Then, the SF-GO carbon aerogels were successfully prepared from the SF-GO cryogels by thermal treatments. Figure 2 shows typical repeating protein amino acid sequences of the silkworm cocoon silk, schematics of the adsorption of the regenerated silk fibroin molecules onto the basal plane of GO and the cryogel structure formed from the silk-fibroin-coated GO after the freeze-drying process. However, during the carbonization process, the amorphous silk fibroin molecules adsorbed on the GO surface were thermally decomposed because of the presence of water molecules between the regenerated

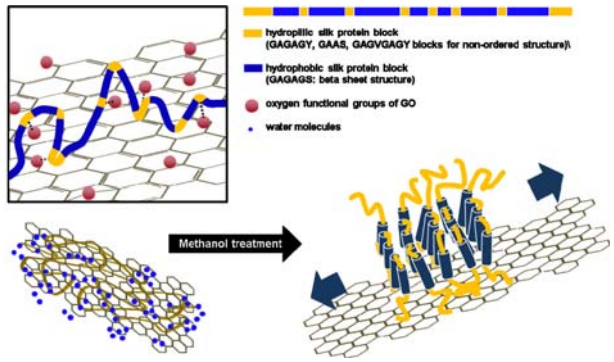

Figure 2. Schematic image depicting interaction between regenerated silk fibroin and GO and crystallization of regenerated silk fibroin molecules.

silk fibroin chains and their amorphous structures. Therefore, the cryogels were treated with methanol vapor and this dehydration method using methanol led to the formation of a β-sheet crystal-dominant structure *via* the intersheet stacking of the hydrophobic silk molecules. This structural transition provided thermo-stabilization to the regenerated silk fibroin, which can be transformed to carbon materials. Figure 3 shows the morphologies of the cryogels with different GO and silk fibroin weight ratios. With increased silk fibroin content, the morphologies of the cryogels dramatically changed and were similar to silk fibroin-based cryogels without GO.[8] Silk-fibroin-dominant samples (*i.e.*, cryogel-4:6 (Figure 3(c)) and cryogel-2:8 (Figure 3(d)) exhibited more dense morphologies than others. In contrast, the cryogel 8:2 sample, a GO-dominant sample (Figure 3(a)), exhibited loosely assembled structures of separate nanoplates. This result suggested the importance of the GO and silk fibroin weight ratio in terms of affecting the morphological and pore characteristics of the cryogels. Figure 4 shows the morphologies of the

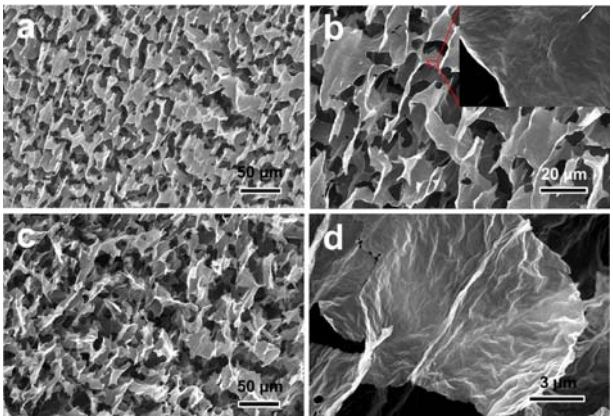

Figure 4. SEM images of (a, b) cryogel-6:4 under different magnifications and (c, d) that of SF-GO carbon aerogels under different magnifications.

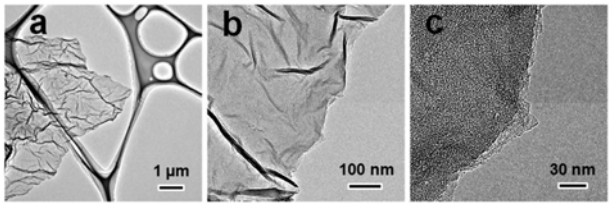

Figure 5. TEM images of different magnifications of carbon nanoplates obtained by ultrasound treatment of SF-GO carbon aerogels in *N*,*N*-dimethylformamide.

cryogel-6:4 sample and the carbonized cryogel-6:4 sample (SF-GO carbon aerogels). The cryogel-6:4 samples exhibited porous interconnected network structures composed of numerous nanoplates (Figure 4(a),(b)). After carbonization, the porous structure was maintained and indeed the structure was rendered even more porous by the loosely assembled carbon nanoplates. In addition, additional winkles on the surface of the carbonized nanoplates were also observed (Figure 4(c),(d)). Figure 5 shows more specific morphologies under different magnifications of the wrinkled carbon nanoplates obtained by ultrasound treatment of the SF-GO carbon aerogels in *N*,*N*-dimethylformamide. Disordered carbon structures were observed on the surface of the sample (Figure 5(c)). This result suggests that carbon materials from regenerated silk fibroins were well-developed on the surface of the samples.

Figure 6 shows the results of characterizing the cryogel 6:4 and SF-GO carbon aerogels by X-ray photoelectron spectroscopy (XPS). The cryogel 6:4 shows numerous nitrogen functional groups such as O=C-N and C-N centered at 400.2 and 400.1 eV, respectively, indicating the presence of silk fibroin on the surface of the cryogel 6:4 (Figure 6(a) and (b)). Also, a large amount of oxygen functional groups were found (Figure 6(a) and (c)). The oxygen groups could be originated from both silk fibroin and G-O. In the C 1s XPS profile of the carbon aerogel, several distinct peaks (C-O and C-N centered at 285.5 eV and C(O)O centered at 288.7 eV) were observed in addition to a main C-C peak at 284.5 eV (Figure 6(d)). The nitrogen atoms in the SF-GO carbon aerogels were observed to belong to two groups and were in the form of pyridinic and pyrrolic/pyridone moieties, as indicated by the N 1s peak centered at 397.7 and 400.0 eV, respectively (Figure 6(e)). The presence of nitrogen groups in the SF-GO carbon aerogels suggests that the regenerated silk fibroins were successfully transformed to carbonaceous materials. Also, the two distinct peaks in the O 1s profile indicated that the oxygen atoms were present in the form of carbonyl groups (531.4 eV) and various other oxygen groups (533.7 eV) (Figure 6(f)). These surface functional groups can be expected to affect the electrochemical performances of the carbon materials through pseudocapacitive effects.[16,25,33-37] The Raman spectrum of the SF-GO carbon aerogels is exhibited in Figure 7(a). The peak positions of the *D*, *G*, and 2*D* bands were measured as ~1363, ~1600, and ~2744 cm^{-1}, respectively.

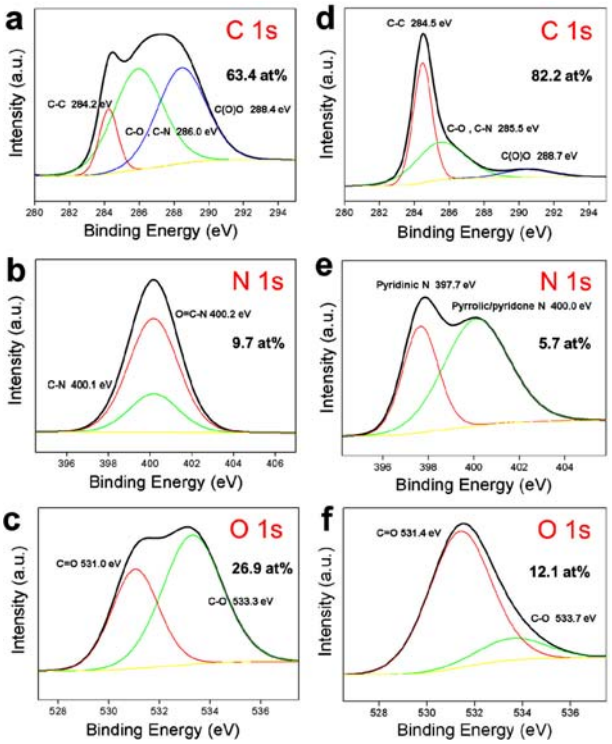

Figure 6. XPS profiles of (a) C 1*s*, (b) N 1*s*, and (c) O 1*s* acquired from cryogel-6:4, and (d) C 1*s*, (e) N 1*s* and (f) O 1*s* of SF-GO carbon aerogels.

The values were similar to that indicated in a previous report.[16] Further, the ratio of the *D* peak intensity to the *G* peak intensity ($I_G I_D^{-1}$) was calculated as ~0.83. The size of the crystal domain could be measured from the $I_G I_D^{-1}$ using the equation $I_D I_G^{-1}=C(\lambda)L^{-1}$, where *L* is the size of the graphene nanoflakes and C=4.4 nm for λ=514.5 nm.[38] From these values, the size of the graphene nanoflakes was measured as 5.3 nm. The X-ray diffraction (XRD) data showed a (002) diffraction peak (26.1°), corresponding to the degree of stacking order of the carbon layer structure. Another diffraction peak was observed at 42.8°, corresponding to the presence of an (100) ordered hexagonal structure (Figure 7(b)). Also, a broad peak was observed at approximately 18°, which could be attributed to an amorphous carbon structure formed from the regenerated silk fibroin. The pore characteristics of the SF-GO carbon

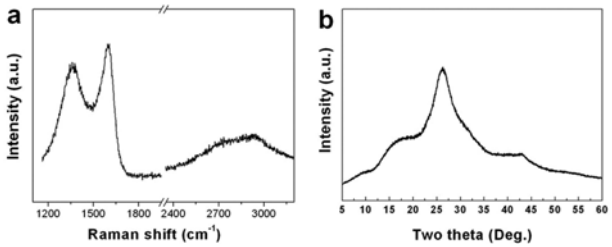

Figure 7. (a) Raman spectrum and (b) XRD pattern acquired from SF-GO carbon aerogels.

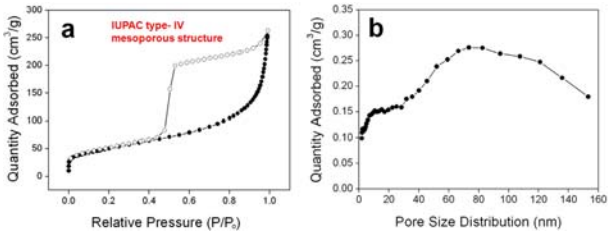

Figure 8. (a) Nitrogen adsorption and desorption isotherm curves and (b) pore size distribution of SF-GO carbon aerogels.

aerogels are shown in Figure 8. The nitrogen adsorption-desorption isotherm curve of the sample showed an IUPAC type-IV mesoporous structure, which exhibited a type of H2 hysteresis loop, indicating a poorly defined pore structure (Figure 8(a)). The specific surface area of the carbon aerogel was calculated as 180.7 $m^2 g^{-1}$ with most of the surface area originating from the mesopores. In addition, the Barrett-Joyner-Halenda (BJH) adsorption average pore diameter was measured as 11.3 nm. The mesopores are thought to originate from the interconnected and crumpled structures of the carbon nanoplate components. The broad pore size distribution of the SF-GO carbon aerogels supports this assumption (Figure 8(b)).

The electrochemical performances of the SF-GO carbon aerogels were analyzed in an aqueous electrolyte (1 M H_2SO_4). Figure 9(a) shows the cyclic voltammograms of the carbon aerogels at scan rates of 5, 10, 20, and 50 mV s^{-1}. The cyclic voltammogram curve at a scan rate of 50 mV s^{-1} exhibited a typical capacitive behavior with rectangular voltammetry characteristics. When the scan rates were decreased, the cyclic voltammogram curves exhibited humps as well as a rectangular shape, indicating that the capacitive response was induced from a combination of the electrical double-layer formation and redox reactions related to the heteroatom functionalities present in the materials. The galvanostatic charge-discharge curves of the carbon aerogels at a current density of 1 A g^{-1} are shown in Figure 9(b). The discharge curve displayed an IR drop owing to the insufficient electrical conductivity of 68×10 S m^{-1} of the SF-GO carbon aerogels. The SF-GO carbon aerogels consist of numerous heteroatoms, which induce unfavorable effects toward electrical conductivity; however, the heteroatoms could also contribute to the specific capacitance. The slope of the discharge curve was altered at approximately 0.6 V, indicating the existence of pseudocapacitive effects. This result coincides with the results observed by cyclic voltammetry. The SF-GO carbon aerogels were found to possess a relatively low specific surface area of 180.7 $m^2 g^{-1}$; nevertheless, their specific capacitance at a current density of 1 A g^{-1} was approximately 260 F g^{-1}. This indicates that the pseudocapacitive effects significantly contributed to the specific capacitance of the SF-GO carbon aerogels. A high specific capacitance of 298 F g^{-1} was achieved on the discharge curve with a constant current of 0.75 A g^{-1} (Figure 9(c)). The value

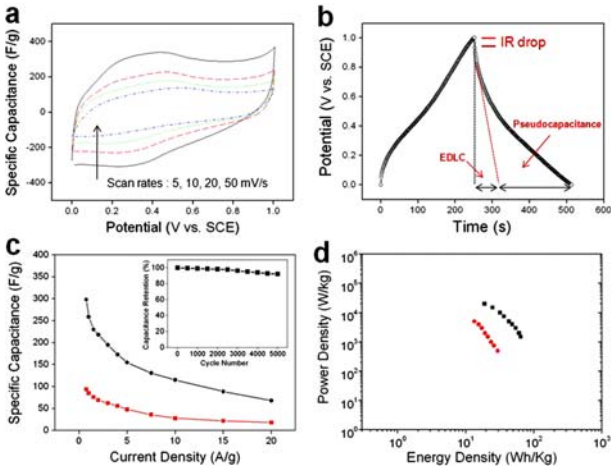

Figure 9. (a) Cyclic voltammograms of SF-GO carbon aerogels at scan rates of 5, 10, 20, and 50 mV s^{-1} over a potential range 0-1 V in 1 M H_2SO_4 electrolyte. (b) Galvanostatic charge/discharge curves of SF-GO carbon aerogels at a current density of 1 A g^{-1} over potential range 0-1 V in 1 M H_2SO_4. (c) Variation of specific capacitance of SF-GO carbon aerogels (black, square) and reduced GO (red, circle) with current density over potential range 0-1 V in 1 M H_2SO_4. Inset indicates capacitance retention during repetitive 5000 charge/discharge cycles. (d) Ragone plot of all SF-GO carbon aerogels and reduced GO-based supercapacitors in 1 M H_2SO_4.

was approximately three times higher than that shown by the reduced GO (94 F g^{-1}), which is fabricated by a similar thermal annealing process used for preparing the SF-GO carbon aerogels. In addition, at a current density of 10 A g^{-1}, the capacitance value of the SF-GO carbon aerogels increased to a value above 100 F g^{-1}. Cycle stabilities of the SF-GO carbon aerogels were characterized during 5000 constant current charge-discharge cycles at a current density of 3 A g^{-1}. After 5000 cycles, the capacitance values decreased to only 7.9% of the initial capacitance, demonstrating the good cyclic stability of the SF-GO carbon aerogels (inset of Figure 9(c)). The energy density and power density reached values of 63 W h kg^{-1} and 20 kW kg^{-1}, respectively (Figure 9(d)). The energy density of the SF-GO carbon aerogels was found to be two times higher than that of the reduced GO (29 W h kg^{-1}).

Conclusions

SF-GO carbon aerogels based on regenerated silk proteins and GO were successfully prepared by a flash-freezing/lyophilization process followed by carbonization. The regenerated silk fibroins were transformed to carbon materials using a methanol vapor treatment. SF-GO carbon aerogels with optimal porous characteristics were obtained by using GO/regenerated silk protein hybrids at a weight ratio of 6:4. The SF-GO carbon aerogels contained numerous heteroatoms with 5.7 at% of nitrogen and 12.1 at% of oxygen. The material exhibited a specific surface area of 180.7 $m^2 g^{-1}$. The SF-

GO carbon aerogels exhibited a high capacitance of 298 F g^{-1} at a current density of 0.75 A g^{-1} because of the pseudocapacitive effects originating from the electroactive heteroatoms. The SF-GO carbon aerogels showed energy and power densities values of 63 W h kg^{-1} and 20 kW kg^{-1}, respectively. The energy density was two times higher than that shown by reduced GO (29 W h kg^{-1}). In addition, the SF-GO aerogels exhibited stability during 5000 constant current charge-discharge cycles.

Acknowledgments. This work was supported by the National Research Foundation of Korea Grant (NRF), funded by the Korean Government (MEST) (NRF-2010-C1AAA001-0029018) and (NRF-2013R1A1A2A10008534).

References

(1) http://faostat3.fao.org.
(2) C. Veparia and D. L. Kaplan, *Prog. Polym. Sci*., **32**, 991 (2007).
(3) S. W. Hwang, H. Tao, D. H. Kim, H. Cheng, J. K. Song, E. Rill, M. A. Brenckle, B. Panilaitis, S. M. Won, Y. S. Kim, Y. M. Song, K. J. Yu, A. Ameen, R. Li, Y. Su, M. Yang, D. L. Kaplan, M. R. Zakin, M. J. Slepian, Y. Huang, F. G. Omenetto, and J. A. Rogers, *Science*, **337**, 1640 (2012).
(4) R. Capelli, J. J. Amsden, G. Generali, S. Toffanin, V. Benfenati, M. Muccini, D. L. Kaplan, F. G. Omenetto, and R. Zamboni, *Org. Electron.,* **12**, 1146 (2011).
(5) C. Müller, M. Hamedi, R. Karlsson, R. Jansson, R. Marcilla, M. Hedhammar, and O. Inganäs, *Adv. Mater.*, **23**, 898 (2011).
(6) H.-J. Jin and D. L. Kaplan, *Nature,* **424**, 1057 (2003).
(7) H.-S. Kim, S. H. Yoon, S.-M. Kwon, and H.-J. Jin, *Biomacromolecules,* **10**, 82 (2009).
(8) S.-M. Kwon, H.-S. Kim, and H.-J. Jin, *Polymer*, **50**, 2786 (2009).
(9) D. Wu, R. Fu, M. S. Dresselhaus, and G. Dresselhaus, *Carbon*, **44**, 675 (2006).
(10) T. P. Fellinger, R. J. White, M. M. Titirici, and M. Antonietti, *Adv. Funct. Mater.*, **22**, 3254 (2012).
(11) J. Biener, M. Stadermann, M. Suss, M. A. Worsley, M. M. Biener, K. A. Rose, and T. F. Baumann, *Energy Environ. Sci.,* **4**, 656 (2011).
(12) M. M. R. Khan, Y. Gotoh, H. Morikawa, M. Miura, Y. Fujimori, and M. Nagura, *Carbon,* **45**, 1035 (2007).
(13) Y. J. Kim, Y. Abe, T. Yanagiura, K. C. Park, M. Shimizu, T. Iwazaki, S. Nakagawa, M. Endo, and M. S. Dresselhaus, *Carbon*, **45**, 2116 (2007).
(14) T. Iwazaki, R. Obinata, W. Sugimoto, and Y. Takasu, *Electrochem. Commun.,* **11**, 376 (2009).
(15) T. Iwazakia, H. Yanga, R. Obinata, W. Sugimoto, and Y. Takasu, *J. Power Sources*, **195**, 5840 (2010).
(16) Y. S. Yun, S. Y. Cho, J. Y. Shim, B. H. Kim, S.-J. Chang, S. J. Baek, Y. S. Huh, Y. S. Tak, Y. W. Park, S. J. Park, and H.-J. Jin, *Adv. Mater.,* **25**, 1993 (2013).
(17) A. K. Geim and K. S. Novoselov, *Nat. Mater.,* **6**, 183 (2007).
(18) S. Stankovich, D. A. Dikin, G. H. B. Dommett, K. M. Kohlhaas, E. J. Zimney, E. A. Stach, R. D. Piner, S. B. T. Nguyen, and R. S. Ruoff, *Nature*, **442**, 282 (2006).
(19) S. Niyogi, E. Bekyarova, M. E. Itkis, J. L. McWilliams, M. A. Hamon, and R. C. Haddon, *J. Am. Chem. Soc.,* **128**, 7720 (2006).
(20) C. Soldano, A. Mahmood, and E. Dujardin, *Carbon*, **48**, 2127 (2010).
(21) M. D. Stoller, S. J. Park, Y. Zhu, J. H. An, and R. S. Ruoff, *Nano Lett.,* **8**, 3498 (2008).
(22) J. J. Yoo, K. Balakrishnan, J. S. Huang, V. Meunier, B. G. Sumpter, A. Srivastava, M. Conway, A. M. N. Reddy, J. Yu, R. Vajtai, and P. M. Ajayan, *Nano Lett.*, **11**, 1423 (2011).
(23) C. Liu, Z. Yu, D. Neff, A. Zhamu, and B. Z. Jang, *Nano Lett.,* **10**, 4863 (2010).
(24) Y. Zhu, S. Murali, M. D. Stoller, A. Velamakanni, R. D. Piner, and R. S. Ruoff, *Carbon,* **48**, 2106 (2010).
(25) H. M. Jeong, J. W. Lee, W. H. Shin, Y. J. Choi, H. J. Shin, J. K. Kang, and J. W. Choi, *Nano Lett.*, **11**, 2472 (2011).
(26) H.-P. Cong, X.-C. Ren, P. Wang, and S.-H. Yu, *ACS Nano*, **6**, 2693 (2012).
(27) H. Hu, Z. Zhao, W. Wan, Y. Gogotsi, and J. Qiu, *Adv. Mater.*, **25**, 2219 (2013).
(28) Z.-S. Wu, S. Yang, Y. Sun, K. Parvez, X. Feng, and K. Mullen, *J. Am. Chem. Soc.*, **134**, 9082 (2012).
(29) S. M. Jung, H. Y. Jung, M. S. Dresselhaus, Y. J. Jung, and J. Kong, *Sci. Rep.*, **3**, 1423 (2013).
(30) X. Zhang, Z. Sui, B. Xu, S. Yue, Y. J. Luo, W. Zhanc, and B. Liu, *J. Mater. Chem.*, **21**, 6494 (2011).
(31) Z. S. Wu, A. Winter, L. Chen, Y. Sun, A. Turchanin, X. Feng, and K. Mullen, *Adv. Mater.*, **24**, 5130 (2012).
(32) Y. S. Yun, Y. H. Bae, D. H. Kim, J. Y. Lee, I.-J. Chin, and H.-J. Jin, *Carbon*, **49**, 3553 (2011).
(33) D. Hulicova-Jurcakova, M. Seredych, G. Q. Lu, and T. J. Bandosz, *Adv. Funct. Mater.*, **19**, 438 (2009).
(34) Y. S. Yun, J. Y. Shim, Y. S. Tak, and H.-J. Jin, *RSC Adv.*, **2**, 4353 (2012).
(35) L. Zhao, L. Z. Fan, M. Q. Zhou, H. Guan, S. Qiao, M. Antonietti, and M. M. Titirici, *Adv. Mater.*, **22**, 5202 (2010).
(36) Y. S. Yun, H. H. Park, and H.-J. Jin, *Materials*, **5**, 1258 (2012).
(37) Y. S. Yun, C. Im, H. H. Park, I. Hwang, Y. Tak, and H.-J. Jin, *J. Power Sources*, **234**, 285 (2013).
(38) A. C. Ferrari and J. Robertson, *Phys. Rev. B*, **61**, 14095 (2000).